ESTUARINE, COASTAL AND SHELF SCIENCE

Editors

N.C. FLEMMING
Institute of Oceanographic Sciences, Wormley, Godalming, Surrey, U.K.

E. NAYLOR
School of Animal Biology, University College of North Wales, Bangor, Gwynedd, North Wales, U.K.

M. GRANT GROSS
Box 1497, Baltimore, Maryland 21203, U.S.A.

Book Review Editor

J.B. WILSON
Institute of Oceanographic Sciences, Wormley, Godalming, Surrey, U.K.

Publication: Monthly
Subscription: Volumes 20–21, 1985
Rate: £127.00 (U.K.)/$315.00 (overseas)

Reprinted from

ESTUARINE COASTAL AND SHELF SCIENCE

ACADEMIC PRESS
London Orlando San Diego
New York Toronto Montreal
Sydney Tokyo

Published by Academic Press Inc. (London) Limited in association with the Estuarine and Brackish-water Sciences Association

Instructions to Authors

(1) *Estuarine, Coastal and Shelf Science* is an international, multidisciplinary journal devoted to the analysis of biological, chemical and physical phenomena occurring in waters from the outer edge of the continental shelf to the upper limits of the tidal zone.

The journal features original papers from such disciplines as zoology, botany, geology, sedimentology, physical oceanography, numerical models and chemical processes. Papers include analysis of species distribution in relation to varying environments; waste disposal, groundwater runoff, estuarine and fjord circulation patterns, physical oceanography and meteorological forcing of semi-enclosed and continental shelf water masses, wave processes and sediment movements.

(2) *Submission of manuscripts*. All manuscripts are to be submitted in English and in the first instance must be sent to one of the three co-editors. All papers concerned with life sciences should preferably be sent to *Professor E. Naylor, School of Animal Biology, University College of North Wales, Bangor, Gwynedd, North Wales, U.K.*, or alternatively, *Dr M. Grant Gross, Chesapeake Bay Institute, The Johns Hopkins University, Baltimore, Maryland, 21218, U.S.A.* Papers primarily concerned with marine physics and earth sciences should be sent to *Dr Nicholas C. Flemming, Institute of Oceanographic Sciences, Wormley, Godalming, Surrey, U.K.*, though papers on sediments or chemistry may also be sent to Dr Grant Gross. Papers submitted to *Estuarine, Coastal and Shelf Science* should preferably be less than 14 printed pages in length, equivalent to 10 000 words without diagrams, or the equivalent in words and diagrams. Major articles up to 15 000 words or equivalent will be accepted at the discretion of the Editors, but there may be a delay in publication of long papers. There are sections for short notes and observations, book reviews, and correspondence.

(3) *Preparation of typescripts*. Typescripts should be submitted in duplicate, using one side only of the paper. Typing should be double spaced throughout the text, including tables, figure legends and reference lists, with a margin of 4 cm on each side. Number consecutively all pages, including title page, abstract, text, references, legends and tables.

(4) *Keywords*. Up to 8 subject-defining Keywords are allocated to each paper immediately preceding the abstract. Authors should select preferred Keywords from the list published in Issue 5 (2), 1977, pp. i-xl and submit them with the Ms if possible. Keywords should be arranged in order of importance, with the geographical or sea area always last.

(5) *Illustrations*. These include figures and plates. Legends for these should be typed in numerical order on a separate sheet, one for figures and one for plates. Illustrations should be designed with the size of the journal page and column in mind. Each illustration should be identified by the name of the author and its number, and its top should be indicated. Magnification should be given by a scale line where appropriate. Unsatisfactory illustrations will be returned to the author. Original illustrations are discarded following publication unless author has requested their return in advance.

Maps, line drawings and diagrams should be prepared with India ink on white drawing paper, tracing paper, or tracing linen. Several drawings grouped on a page as one figure are distinguished as (a), (b), (c), etc. Figures which must be printed larger than page size should be avoided, as they are inconvenient and expensive. Authors may submit original drawings if small enough, or very clear glossy photographs of them. Care should be taken not to overload maps with irrelevant detail, or to use excessive amounts of space to convey little information. The smallest symbols or letters used should not be less than 1·5 mm high after reduction. The author should supply one or two extra copies of each figure suitable for sending reviewers (photocopies, etc. which may be folded).

Plates are page size units, often consisting of several photographs. The plates are numbered consecutively, and individual photographs on a plate are designated (a), (b), (c), etc. Authors should use the minimum number consistent with adequate presentation of the subject. Photographs must be sharp and clear, printed on glossy paper and not smaller than their publication size. They should not be mounted. Copies of photographs for sending to reviewers need not be of the same high quality as the originals, but they must be clear (Xerox copies are usually inadequate).

Tables should be numbered in the order of their position in the text and typed on separate sheets. A brief title should be typed directly above each table.

(6) *References*. In the text, references to the literature cited should list the author's name, year of publication and preferably the specific page numbers in this form: (Smith, 1928, p. 36). Under the heading References cited at the end of the text should be listed all literature cited, double-spaced, arranged alphabetically by authors and chronologically under each author. Initials should be typed after surnames. Publication date should be given directly after the last author. The order should be as follows:

(a) Single authors.

(b) Two authors. References for which there are two authors should be arranged first alphabetically and then chronologically. For text citations, use both author's names and the year. Do not use *et al.* for two-author references.

(c) Three or more authors. References with three or more authors should be arranged chronologically. For all text citations use the surname of the first author only followed by *et al.* and the date.

If more than one reference by the same author or authors published in the same year is cited, use *a, b,* etc., after the year in both text and reference list, e.g. (1963*a*). Journal titles, in reference list should be cited in full. Full title of the paper, journal, volume number and page number should be given.

(7) *Proofs*. Copy editing of manuscripts is performed by the staff of the publishers. The author is asked to check page proofs for typographical errors and to answer queries from the copy editors. No other changes are permitted in proof unless the author is prepared to pay for them.

(8) *Copyright/offprints*. Authors submitting a manuscript do so on the understanding that if it is accepted for publication, exclusive copyright in the paper shall be assigned to the Publisher. In consideration for the assignment of copyright, the Publisher will supply 50 offprints of each paper. Further offprints may be ordered at extra cost at the proof stage. The Publisher will not put any limitation on the personal freedom of the author to use material contained in the paper in other works.

Printed in Great Britain by Henry Ling Ltd., at the Dorset Press, Dorchester, Dorset

Estuarine, Coastal and Shelf Science (1985) **21**, 207–224

A Study of Non-linear Tidal Propagation in Shallow Inlet/Estuarine Systems Part II: Theory[a]

P. E. Speer[b] and D. G. Aubrey

Woods Hole Oceanographic Institution, Woods Hole, MA 02543, U.S.A.

Received 6 June 1984 and in revised form 4 December 1984

Keywords: tidal estuaries; numerical model; non-linear equations; tidal flats; tidal friction; harmonic analysis; U.S.A. east coast

The generation of tidal asymmetries is clarified via numerical integration of the one-dimensional equations for channel geometries characteristic of shallow estuaries. Channels without tidal flats develop a time asymmetry characterized by a longer falling than rising tide. This behavior is enhanced by strong friction and large channel cross-sectional area variability over a tidal cycle. Resulting tidal currents have a shorter, intense flood and a longer, weak ebb (flood-dominant). Addition of tidal flats to the channels can produce a longer rising tide and stronger ebb currents (ebb-dominant), if the area of tidal flats is large enough to overcome the effects of time-variable channel geometry. Weaker friction with flats can also produce this asymmetry.

Despite the physical complexity of these systems, essential features of estuarine tidal response can be recovered from one-dimensional models. Shallow estuaries are shown to have a system response leading to stable, uniform senses of tidal asymmetry (either flood- or ebb-dominated, due to phase-locking of forced tidal constituents), with down-channel development in magnitude of asymmetry. These concepts are illustrated by modeling idealized representations of tidal channels at Nauset Inlet, MA, and Wachapreague Inlet, VA, which have flood- and ebb-dominance, respectively.

Introduction

The tidal response of shallow inlet/estuarine systems commonly found on the U.S. east and Gulf coasts is characterized by the development of asymmetries in the estuarine tide. These asymmetries take the form of unequal duration and/or unequal magnitude of ebb and flood. This distortion of the estuarine tide can be represented by the non-linear growth of harmonics of the astronomical tidal constituents. Some inlet/estuarine systems (e.g. Murrels Inlet, SC, Boon & Byrne, 1981; Nauset Inlet, MA, Aubrey & Speer, 1983) are characterized by longer ebbs than floods and consequently a tendency for higher current velocities during flood (flood-dominant). Other systems (e.g. Wachapreague Inlet, VA, Boon & Byrne, 1981; North Inlet, SC, Nummedal & Humphries, 1978; Price Inlet, SC, FitzGerald & Nummedal, 1983) show the opposite duration asymmetry and

[a] Woods Hole Oceanographic Institution Contribution No. 5691.

[b] Present address: Center for Naval Analyses, Alexandria, VA 22311, U.S.A.

0272–7714/85/080207 + 18 $03.00/0

hence a tendency for stronger ebb currents (ebb-dominant). The different senses of asymmetry have important implications for estuarine sediment transport, dispersal of water column contaminants, and (over long time scales) estuarine/inlet stability.

Some investigators of shallow inlet/estuarine systems have suggested that duration asymmetries are controlled by the variation in estuarine surface area relative to inlet cross-sectional area (e.g. Nummedal & Humphries, 1978; FitzGerald & Nummedal, 1983). The argument is stated utilizing a spatially integrated form of the continuity equation and ignores the role of momentum effects in generating tidal asymmetries. This paper focuses on the generation of tidal asymmetries by non-linear terms in both continuity and momentum. The dynamics of estuarine tidal distortion are described through a series of numerical experiments, based on idealized estuarine geometries.

For representative systems, the estuary is serviced by a narrow inlet and consists of a number of channels generally terminating in bays. The bays may consist largely of tidal flats or may be basins deeper than the connecting tidal channels. Separating the tidal channels are regions of flats exposed at low tides and islands of marsh grass which are occasionally overtopped at high tide. Typical channel depths, h, are 1–10 m and lengths, L, are of the order of 1–10 km. Characteristic values for the tidal amplitude, a, suggest that finite amplitude effects (as indicated by the ratio, a/h) are important in these systems. Since the tidal wavelength, $2\pi/k$, is much greater than L, characteristic length scales are determined by estuarine geometry. The channels are long compared to their width, $b/L \ll 1$, and the horizontal aspect ratio, h/b, is small. The flow may therefore be termed one-dimensional, although channel bends will produce locally two-dimensional effects (e.g. Aubrey & Speer, 1984).

Estuaries addressed in this study are also characterized by a well-mixed water column and negligible freshwater inflow. Mixing is promoted by strong currents (order $1\ \mathrm{m\ s^{-1}}$) often found in estuarine channels, and by interaction of currents with a rough bed. In deeper basins at channel terminations, weak stratification develops during summer months.

The offshore astronomical tide is composed of a discrete number of important constituents. Non-linear interaction between these constituents is possible in a shallow estuary. Field observations of estuarine tides often indicate a rich spectrum of forced motions (e.g. Aubrey & Speer, 1985) ranging from high frequency (i.e. greater than semi-diurnal) to low frequency (e.g. fortnightly). The M_2 constituent, as the major constituent along the north-east U.S. coast, dominates non-linear processes within the estuary. This domination can be shown from theoretical arguments (e.g. Gallagher & Munk, 1971) as well as field observations (Aubrey & Speer, 1983). The harmonics of M_2 are larger than compound tides produced by interaction among constituents.

Field observations (e.g. Boone & Byrne, 1981; Aubrey & Speer, 1984*b*) and theoretical work (e.g. Kreiss, 1957; Dronkers, 1964; Pingree & Griffiths, 1979) have shown that the interaction of M_2 and its first harmonic, M_4, explains the general features of observed tidal asymmetries. The type of tidal distortion (flood-dominant *vs.* ebb-dominant) depends on the relative phasing of M_4 to M_2. Defining the M_2 and M_4 constituents (sea surface or velocity) as

$$A_{M_2} = a_1 \cos(\omega_1 t - \theta_1)$$
$$A_{M_4} = a_2 \cos(\omega_2 t - \theta_2),$$

the relative M_2–M_4 phase is:

$$\Phi = 2\theta_1 - \theta_2.$$

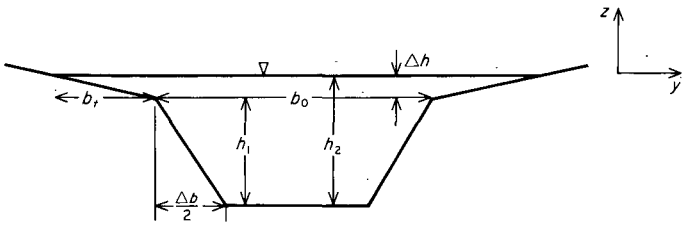

Figure 1. Channel geometry with tidal flats included. $\zeta(x,t)$ is the sea surface elevation at point x and time t.

Model formulation

A trapezoidal geometry is used to represent estuarine channels where width generally increases with elevation above the bottom (Figure 1). We consider the tidally driven problem and focus on common cases where sea level fluctuations, a, are of the same order as the water depth, h (e.g. Kjerfve, 1975).

One-dimensional equations of motion assume hydrostatic pressure, level sea surface across channel, small horizontal aspect ratio ($h/b \ll 1$), and long, narrow channels ($b/L \ll 1$). In real estuaries, these assumptions will be violated locally. Channels with large bedforms and shallow depths may depart from purely hydrostatic conditions. Strong channel curvature (e.g. flow around bends) may violate assumption two. This two-dimensional effect is generally localized, affecting secondary circulation, shear stress and sediment transport patterns in the vicinity of the bend (Smith & McLean, 1983). The present work examines the response to tidal forcing of the entire estuarine channel. Assumptions 3 and 4 hold for many estuaries of interest.

The model dynamics are expressed in terms of cross-sectional flux $U(x,t)$, cross-sectionally averaged velocity $\overline{u}(x,t)$, and sea surface elevation, $\zeta(x,t)$. The equations of motion governing one-dimensional flow are:

$$\frac{\partial \zeta}{\partial t} + \frac{1}{b}\frac{\partial}{\partial x} U = 0 \tag{1}$$

$$\frac{\partial U}{\partial t} + \frac{\partial}{\partial x}\frac{U^2}{A} = -gA\frac{\partial \zeta}{\partial x} - \frac{\tau_b}{\rho} P \tag{2}$$

where τ_b = average shear stress on solid boundaries, P = wetted perimeter; A = channel cross-sectional area, and b = channel width.

The friction term in (2) includes sidewall friction by considering channel sidewalls in the wetted perimeter. The problem is closed mathematically by formulating friction as follows:

$$\tau_b = \frac{\rho f |U| U}{A \cdot A} \tag{3}$$

where f = dimensionless friction factor. Principal non-linear effects in equations (1), (2) and (3) enter through quadratic friction, advection of momentum, and tidal interactions with estuarine geometry in the continuity equation.

Important physical elements of these systems are tidal flats, which can occupy a significant fraction of the total estuarine surface area (e.g. FitzGerald & Nummedal, 1983). They may be incised with shallow channels which are active during only a portion of the tidal cycle. Obviously, a one-dimensional model cannot handle the presence of several distinct channels across a channel section. Throughout most of the estuary, however, tidal flats serve mainly to store water as opposed to transporting momentum. Since bottom friction substantially weakens the velocity as water moves away from the main channel onto the flats, an approximation of the effect of tidal flats can be included solely in the continuity equation. This idealization neglects dissipation of the tide as water flows across the flats, as well as the dissipative effect of low velocity fluid draining into the ebbing channel flow from tidal flats during falling tide. The latter effect can be modeled by including a lateral inflow term in the momentum equation (e.g. Dronkers, 1964; Speer, 1984).

A model estuarine channel is composed of a momentum transporting portion of maximum width, b_0, and a storage region of initial width, $2b_t$ (Figure 1). The slope of the storage region, $\tan\theta$, is equal to $\triangle h/b_t$, where $\triangle h$ represents the difference between total channel depth and the depth at width b_0. The effects of tidal flats enter through the continuity term, $(1/b)\,\partial U/\partial x$, where b is the total width including flats. Equations (1) and (2) constitute an initial-boundary value problem with initial conditions:

$$U(x,0) = 0$$
$$\zeta(x,0) = 0$$

Boundary conditions include a condition of no flux into solid boundaries and a specified forcing at the channel open boundary:

$$U(L,t) = 0$$
$$\zeta(0,t) = a\cos\omega t$$

Boundary forcing for the problem consists of the M_2 constituent. In principle, the modeling can include an input spectrum consisting of the other important astronomical constituents (e.g. O_1, K_1, S_2, N_2). However, many features of estuarine channel response to tidal forcing are revealed by concentrating on M_2. Ter-diurnal compound constituents (e.g. MK_3, MO_3) do not produce duration asymmetry, and quarter-diurnal compound constituents (e.g. MS_4, MN_4) have smaller amplitudes than M_4 (Aubrey & Speer, 1985).

Numerical integration of equations (1) and (2) is carried out with an explicit time-stepping finite difference model (e.g. Teubner & Noye, 1978; Prandle, 1980; Uncles & Jordan, 1980; Speer, 1984). Sea surface and transport are spatially staggered with width and depth defined at sea surface grid points. Time derivatives are replaced by forward time steps, spatial derivatives by centered differences. The model uses 28 grid points along channel. The accuracy and stability of the numerical scheme is discussed in Speer (1984). The formal accuracy of the numerical scheme is approximately $0(\triangle t, \triangle x^2)$. The procedure in model runs was to time-step a particular experiment until a periodic solution was obtained. Amplitudes and phases of harmonics (sea surface and velocity) were determined by harmonic analysis of the solutions for $\overline{u}$ and ζ. Additionally, terms in the equations of motion were harmonically analysed to examine mechanisms for particular cases of non-linear tidal distortion (Speer, 1984).

Results

Numerical experiments conducted in this study fall into two classes:

(1) Tidal propagation in channels with constant mean width and depth (along the length of the channel), both with and without flats.

(2) Tidal propagation in channels with geometries characteristic of two real estuaries.

Each experiment was examined for the sense of tidal asymmetry, and for the phasing and rate of growth of harmonics, particularly the first harmonic (M_4).

The first class of numerical experiments is similar in philosophy to a number of analytical efforts which have examined aspects of tidal propagation in channels (e.g. Kreiss, 1957; Gallagher & Munk, 1971; Kabbaj & Le Provost, 1980). Previous examples are limited to cases of simple constant width and depth *rectangular* channels, and the ratio $a/h \ll 1$. In fact, as previously discussed, natural estuarine channels tend to have widths which vary with depth. To include this feature, cases where a/h is not constrained to be much less than one, and the presence of tidal flats, numerical integration of the equations is necessary.

The second class of experiments adds features characteristic of natural estuarine systems. These experiments compare two inlet/estuarine systems (Nauset Inlet, MA and Wachapreague Inlet, VA) with different tidal responses. Nauset Inlet is characterized by strong harmonic growth, particularly of the M_4 constituent, and an asymmetry favouring longer ebbs than flood (e.g. Aubrey & Speer, 1983, 1985). Wachapreague Inlet has much weaker harmonic growth and an asymmetry favoring longer floods (e.g. Byrne *et al.*, 1977; Boon & Byrne, 1981). Each estuary is modeled by an idealized channel which represents its basic geometry.

The geometry of model runs can be described by a number of non-dimensional parameters. Since channel lengths are much smaller than tidal wavelengths ($Lk/2\pi \ll 1$) for the estuaries of interest, longitudinal length scales are not an important parameter. Characteristic values of the ratio a/h range from 0·1 to 0·5 for the estuaries of interest. An 'amplitude dispersive' behavior in shallow water waves with a cascade of energy into harmonics of the fundamental frequency is anticipated for this range of values (e.g. Gallagher & Munk, 1971).

Variation in channel cross-sectional area and width over a tidal cycle is described by the ratios a/h and $\triangle b/b$, shown by expressions for cross-section area, A, and width, b, for a trapezoidal channel (without tidal flats):

$$A = A_0 + b_0 \cdot \zeta \left(1 + \frac{1}{2}\frac{\triangle b}{b_0} \cdot \frac{\zeta}{h_2}\right) \tag{4}$$

A_0 = channel area at mean depth h_2

$$b = b_0\left(1 + \frac{\triangle b}{b_0} \cdot \frac{\zeta}{h_2}\right) \tag{5}$$

Strong modulation of both channel area and width for non-rectangular geometries occurs if the ratio $\triangle b/b_0$ is large. No variability occurs in width, of course, for the rectangular case. For the non-rectangular case and a simple harmonic tide, cross-sectional changes will contain both the original frequency and its first harmonic at $0(a/h)$, suggesting that time variable geometry may be an important source of harmonic growth. Because cross-sectional area and channel perimeter change at different rates over a tidal cycle, friction effects may be strongly modulated by geometry.

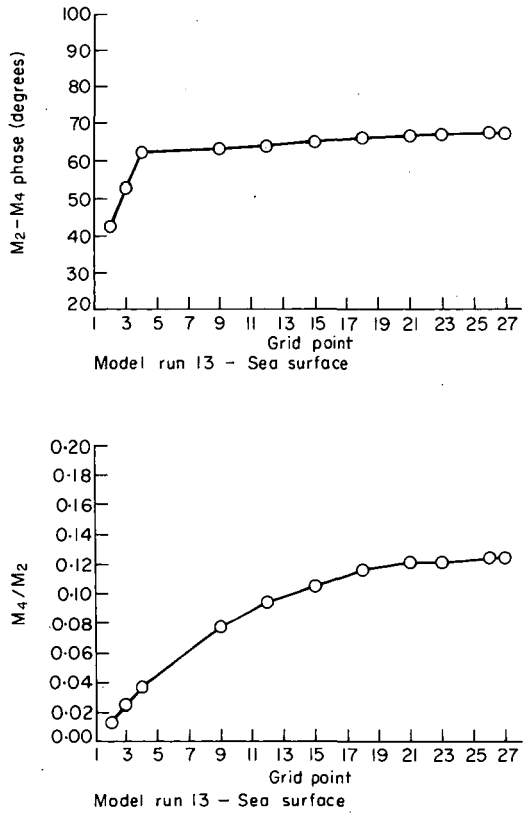

Figure 2. Pattern of M_4 growth in sea surface and relative M_2–M_4 phase in sea surface for a numerical experiment without tidal flats. Note the rapid phase adjustment within the first five grid points.

The geometry of tidal flats is described by the slope of the storage banks, tan θ. Also the parameter (A_f/A_c), comparing the fractional change in the cross-sectional storage area (A_f) *vs.* momentum transporting portion of the channel (A_c) describes the channel geometry with tidal flats:

$$\frac{A_f}{A_c} = \frac{2+a}{\triangle h}\left(\frac{b_0}{b_t}\right)^{-1}$$

Constant mean width/depth problems

Both channels with and without tidal flats are considered. Harmonic growth depends on the balance between energy extracted from the fundamental frequency by non-linear friction, advection and continuity, and the energy lost to dissipation. For these geometries, friction and advection of momentum are strongest near the forcing boundary, however advection is relatively unimportant as an M_4 generation mechanism compared to friction. In contrast to friction and advection, the magnitude of non-linear continuity shows only a slow decline (if any) downchannel. Near the interior boundary little change occurs in the growth of harmonics in sea surface, and harmonics in velocity decrease to zero. Model runs reach an ' equilibrium ' phase relationship between M_2 and M_4 in both sea surface and velocity (or transport) which is determined by the channel

TABLE 1. Channels without tidal flats: results of numerical experiments

Expt.	a/h	$\triangle b/b_0$	$a/h \cdot \triangle b/b_0$	f	M_4/M_2[a]	M_4/M_2[b]	Φ_ζ[c]	Φ_u[d]	$\% \triangle H$[e]
10B	0·22	0	—	0·02	0·005	0·016	92	75	0
10	0·32	0	—	0·02	0·019	0·065	81	50	0
10A	0·32	0	—	0·00	0·002	0·010	117	84	0
10C	0·39	0	—	0·02	0·019	0·065	79	55	0
10D	0·46	0	—	0·02	0·027	0·092	74	48	0
22	0·32	0·20	0·06	0·02	0·021	0·073	76	42	1
24	0·32	0·27	0·09	0·02	0·022	0·076	75	38	1
24A	0·32	0·27	0·09	0·01	0·013	0·046	85	59	0
24B	0·32	0·48	0·15	0·02	0·026	0·093	72	26	4
13G	0·20	0·75	0·15	0·02	0·009	0·031	85	56	0
13B	0·26	0·75	0·20	0·02	0·021	0·074	78	31	3
13	0·32	0·75	0·24	0·02	0·037	0·124	68	11	10
13E	0·32	0·75	0·24	0·01	0·026	0·092	75	29	3
13F	0·32	0·75	0·24	0·00	0·008	0·026	101	73	0
13A	0·32	0·87	0·28	0·02	0·044	0·140	65	4	16
13C	0·39	0·75	0·29	0·02	0·040	0·132	70	17	8
13D	0·32	0·94	0·30	0·02	0·050	0·150	65	2	19
13I	0·32	0·94	0·30	0·002	0·014	0·047	93	62	0
13J	0·43	0·75	0·32	0·02	0·056	0·168	64	3	7

[a]Sea surface amplitude ratio at grid point 4 (1 km).
[b]Sea surface amplitude ratio at grid point 26 (6·5 km).
[c]Sea surface M_2–M_4 relative phase at grid point 26.
[d]Velocity M_2–M_4 relative phase at grid point 26.
[e]% decline in tidal range at grid point 28 (7 km).

geometry and magnitude of friction in the channel. A representative model run (Figure 2) shows rapid adjustment in sea surface M_2–M_4 phase, Φ_ζ, near the forcing boundary followed by more gradual changes near the interior boundary. The ratio of sea surface M_4 to M_2 amplitude, $(M_4/M_2)_\zeta$, also increases rapidly near the forcing boundary before leveling off near the interior boundary.

Differences exist between the model behavior described above and that of natural estuarine channels. Cross-sectional area can vary widely along real channels producing large velocities well within the estuary. As a result, friction and advection will not necessarily show the monotonic downchannel decline exhibited by the models. The advective term, although relatively unimportant in these models, can become locally significant in natural channels due to rapid changes in geometry (e.g. flow around bends, sudden channel expansions). It can, in fact, dominate friction as an M_4 generation mechanism in deeper channels with different geometries than those under consideration. Pingree and Maddock (1978) have shown, for example, that the advective term is more important than friction for M_4 generation in the English channel.

Channels without tidal flats

Numerical experiments are presented in terms of increasingly time variable channel cross-sectional area as shown by the parameter, $a/h \cdot \triangle b/b_0$ (Table 1). This non-dimensional parameter is strictly geometrical, indicating the variability of channel cross-section area over a tidal cycle. Since channel area enters into both dynamical terms and the non-linear continuity term, a large value of this parameter can indicate the possibility of a strongly non-linear tidal response. It is not, however, a fundamental measure of the

non-linearity of the long wave (or shallow water) equations, which is provided by the ratio of wave particle velocity, u, to wave phase velocity, c. For long waves, this ratio equals a/h, the non-dimensional wave amplitude. The condition of linearity for long waves requires that $u/c \ll 1$. If the ratio is small, a large value of $\triangle b/b_0$ will have no impact on the non-linear development of the tide. Because a/h is large for these examples, channel geometry will influence the tidal response.

All model runs produced time asymmetries characterized by a longer falling than rising tide. The maximum time asymmetry of this type for a given ratio $(M_4/M_2)_\zeta$, is produced by an M_2–M_4 relative phase, Φ_ζ of $+90°$. As shown in Table 1, Φ_ζ ranges approximately 30° on either side of 90°, The sense of time asymmetry is determined by the M_2–M_4 phase, and its magnitude by the M_4/M_2 ratio. Results from the experiments show $(M_4/M_2)_\zeta$ depends strongly on geometry and friction characteristics of the channel. In general, more time-variable geometry and strong friction produce larger M_4/M_2 ratios. The increase in this ratio is dominated by growth in M_4 as opposed to a decrease in M_2.

These numerical examples also produce little decline in tidal range except for cases of strongly time-variable channel cross-section area (e.g. experiments 13, 13A, 13D). This behavior is expected considering the linear problem (e.g. Dronkers, 1964), which shows friction in a rectangular channel is not effective in reducing tidal amplitude over the short channel length scales considered.

Mean velocity exhibits more variability in M_2–M_4 phase than does sea surface. If M_4 is in phase with M_2 in velocity ($\Phi_u \simeq 0°$), the case of short, strong floods versus long, slow ebbs occurs (e.g. experiments 13A, 13D). From a strict continuity argument, this situation results when falling tide exceeds rising tide in duration. Experiments approximating this phase relationship are characterized by both strong friction *and* time variable channel geometry. All cases showed greater harmonic growth in velocity than in sea surface (i.e. large M_4/M_2 ratios). Experiment 13 (Table 1, Figure 3) shows that whereas M_4 steadily grows in amplitude for sea surface, it first increases and then declines in mean velocity. Initially, non-linear processes pump more energy into this harmonic than is removed by friction. Eventually, dissipation and the constraint on velocity imposed by the interior boundary condition reduce its amplitude.

Effect of channel geometry on sea surface response is clarified by three experiments (Figure 4, frequency domain; Figure 5, time domain) arranged in order of increasing cross-sectional variability over a tidal cycle. Each experiment has the same friction factor ($f = 0{\cdot}02$) and tidal forcing ($a/h = 0{\cdot}32$). Friction and flow-geometry interactions produce an increasingly non-linear response as channel cross-sectional area becomes more time-variable. The phase relationship between M_2 and M_4 in each case (Table 1) leads to falling tide exceeding rise tide in duration, with the asymmetry increasing downchannel. The distortion of the tide at the model's interior boundary for three examples (Figure 6) shows: (i) the duration of rising tide decreases with increasing $\triangle b/b_0$; (ii) greater reduction in tidal range associated with increasingly trapezoidal geometry; and (iii) the tendency towards increased (though small) set-up (tidally-averaged) in sea surface with increasingly trapezoidal geometry. The greater the dissipation of the tide, the larger the set-up in mean sea level at the channel interior boundary.

Since channel cross-sectional variability over a tidal cycle is a function of a/h, increasing this ratio leads to a more distorted tide. Similar to the geometry parameter $\triangle b/b_0$, larger values of a/h lead to stronger harmonics in cross-sectional area and width. A comparison of the results of experiments 24B and 13G (Table 1) emphasizes that a/h

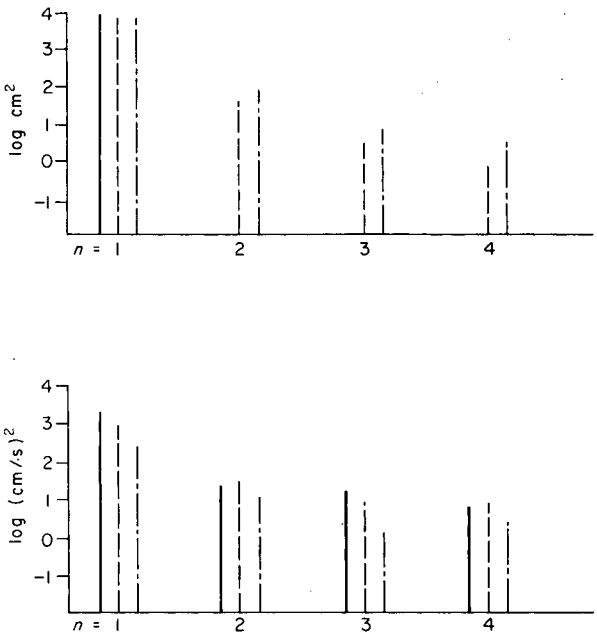

Figure 3. Periodogram derived from harmonic analysis of numerical solution for model run 13. Top panel is sea surface at three grid points, bottom is velocity at the same points. The numbers along the horizontal axis refer to M_2 and its harmonics (i.e. $1 = M_2$; $2 = M_4$; $3 = M_6$; $4 = M_8$). ——, grid point 1; – – –. grid point 9; — · —, grid point 18.

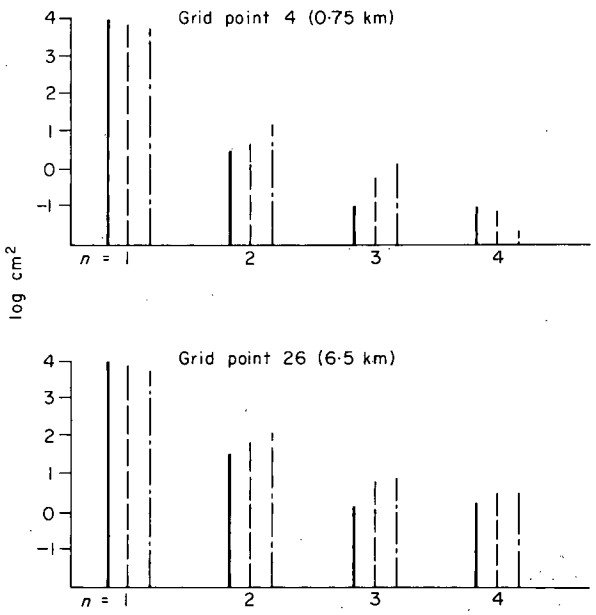

Figure 4. Periodogram of sea surface for three model runs at two different grid points. These experiments illustrate the effect of channel geometry (variability increasing in order of experiments 10, 24B, 13D) on sea surface tidal distortion. ——, experiment no. 10; – – –, 24B; — · —, 13D.

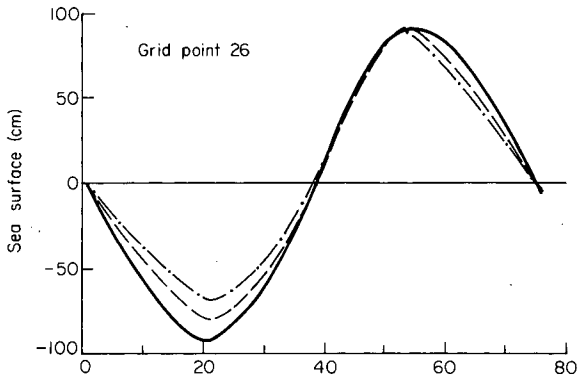

Figure 5. Distortion of the sea surface tide near model's interior boundary for the three experiments shown in Figure 4. ——, experiment no. 10; – – –, 13; — · —, 13D.

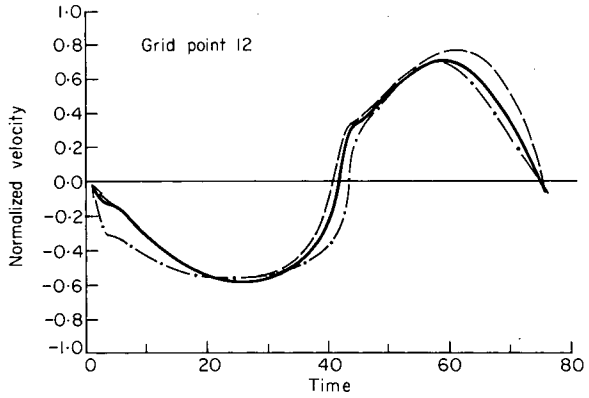

Figure 6. Distortion of velocity as a function of channel geometry. The velocity for each numerical experiment is normalized by the maximum velocity developed in that model run. – – –, experiment no. 10; ——, 24; — · —, 13D.

exerts a fundamental control on non-linearity in estuarine tidal response. Although the two experiments have approximately the same value of the parameter, $a/h \cdot \triangle b/b_0$, experiment 24B has the larger a/h ratio and consequently the more non-linear tide. Channel geometry effects are only important if a/h is sufficiently large.

Most of the experiments were run with friction factors of $0(10^{-2})$. Estimates of friction factors in shallow estuaries with strong tidal flows, large bedforms, and high sediment transport rates are of this magnitude (e.g. Swift & Brown, 1983; Speer & Aubrey, in prep.). Distortion of the tide at the model's interior boundary as a function of friction (Table 1: experiments 13I, 13E, 13) shows a pattern similar to that produced by increasing the magnitude of the geometry parameter. Friction factors of $0(10^{-5})$ cause negligible tidal decay and produce little harmonic growth in the short channels under consideration, even for strongly trapezoidal geometries (experiment 13I).

It has been stated that quadratic friction produces only odd harmonics (i.e. M_6) and that even harmonics (i.e. M_4) are produced by non-linear continuity and advection (e.g. Hamilton, 1978). Analytical models employing perturbation schemes to include quadratic friction find odd harmonics generated by friction to second order in non-dimensional wave amplitude if a time-invariant friction factor is used (e.g. Gallagher & Munk, 1971; Kabbaj & Le Provost, 1980):

$$\overline{U} = \varepsilon \cos\omega t \tag{6a}$$

$$\overline{U}|\overline{U}| = \frac{8}{3\pi}\varepsilon^2 \{\cos\omega t + \tfrac{1}{5}\cos 3\omega t - \ldots .\} \tag{6b}$$

where ε represents a non-dimensional measure of current amplitude. Higher order interactions [i.e. $0(\varepsilon^3)$] between the fundamental frequency and its harmonics are not calculated in analytical models. In fact, as Gallagher and Munk (1971) point out, the even harmonics can be modified considerably by higher order frictional interactions. Numerical results presented here and those of other numerical experiments (e.g. Pingree & Maddock, 1978; Prandle, 1980) show the importance of friction in generating both even and odd harmonics. This is important because even harmonics (M_4) produce the time asymmetries.

Increased channel cross-section variability, non-dimensional tidal forcing and friction also lead to an increasingly distorted mean velocity. Increasing the geometry parameter, $a/h \cdot \triangle b/b_0$, while keeping friction constant, increases the magnitude asymmetry and the duration of ebb (Figure 6). The experiments with a phase, Φ_u, approximately zero are also characterized by the strongest harmonic growth in sea surface and longest falling tides.

Harmonic analysis of non-linear terms reveals that friction and continuity are responsible for producing the tidal asymmetry. The advective term is small compared to friction and not an important driving mechanism for M_4 in these models. In general, the M_4 acceleration from friction is at least an order of magnitude larger than that from advection. The momentum balance (and hence tidal distortion) for these model runs is dominated by friction and pressure gradient as is typical in these systems.

Both friction and time-varying geometry terms drive the sea surface phase relationship (Φ_ζ) to approximately $+90°$ or less. Strong friction and time-variable geometry produce a sea surface phase of $\sim 65°$ and velocity phase $\sim 0°$, as well as strong harmonic growth. Reducing friction for the same variable geometry changes phase relationships dramatically. Similarly, making the geometry less variable while keeping the same friction causes large phase changes. Both changes also have the effect of reducing harmonic growth (see Speer, 1984).

Channel with tidal flats

These experiments add tidal flats to some of the channel geometries previously described (Table 2). The manner in which tidal flats are introduced causes a discontinuity in the channel geometry with a sharp break between transported and stored fluid. Three geometries from the first group of experiments (10, 13, 13A) were utilized to assess the effects of tidal flats. The experimental results both in terms of phase and harmonic growth show a different pattern than the previous examples. In general, patterns of harmonic growth are more complex for these cases (the complexities will be discussed later), but certain trends can be derived.

In some of the experiments, the relative sea surface phase, Φ_ζ, is greater than $+180°$, indicating a *longer rising tide* than falling tide (and contrasts with the previous experiments). The channel characteristics include lower time-variability in channel cross-section and larger values of A_f/A_c (area of flats/area of channel). In general, trapezoidal channels with relatively small tidal flats show phases, Φ_ζ, between $+100°$ and $+180°$, indicating a *longer falling tide*. All experiments show a greater adjustment in Φ_ζ than the previous experiments. In every example, falling tide exceeds rising tide in duration near

TABLE 2. Channels with tidal flats: results of numerical experiments

Expt.	a/h	$\triangle b/b_0$	$a/h \cdot \triangle b/b_0$	tanθ	A_f/A_c	f	M_4/M_2[a]	M_4/M_2[b]	Φ_ζ[c]	Φ_u[d]	$\% \triangle H$[e]
11	0·32	0		0·0025	4·41	0·0200	0·073	0·265	207	215	12
12	0·32	0		0·0025	4·41	0·0100	0·071	0·242	217	225	2
11B	0·32	0		0·0050	2·60	0·0200	0·046	0·166	209	223	4
11A	0·32	0		0·0075	2·00	0·0200	0·033	0·114	213	231	2
25	0·39	0		0·0025	4·41	0·0200	0·068	0·248	199	216	25
25A	0·45	0		0·0025	4·41	0·0200	0·080	0·226	192	232	36
14A	0·32	0·75	0·24	0·00125	5·00	0·0200	0·072	0·251	193	222	45
14	0·32	0·75	0·24	0·0025	2·75	0·0200	0·085	0·175	182	279	30
14B	0·32	0·75	0·24	0·0025	2·75	0·0100	0·064	0·174	193	236	13
14C	0·32	0·75	0·24	0·0025	2·75	0·0075	0·056	0·171	199	230	7
17	0·32	0·75	0·24	0·0075	1·25	0·0200	0·055	0·075	131	332	16
19	0·32	0·75	0·24	0·0075	1·25	0·0100	0·031	0·053	144	310	8
17B	0·32	0·75	0·24	0·0150	0·62	0·0200	0·033	0·085	81	345	7
23A	0·28	0·875	0·245	0·0075	1·08	0·0200	0·039	0·060	128	329	14
23	0·32	0·875	0·28	0·0075	1·25	0·0200	0·064	0·085	117	336	21
23B	0·32	0·875	0·28	0·0025	2·75	0·0200	0·089	0·162	167	309	38

[a]Sea surface amplitude ratio at grid point 4 (1 km).
[b]Sea surface amplitude ratio at grid point 26 (6·5 km).
[c]Sea surface M_2–M_4 relative phase at grid point 26.
[d]Velocity M_2–M_4 relative phase at grid point 26.
[e]% decline in tidal range at grid point 28 (7 km).

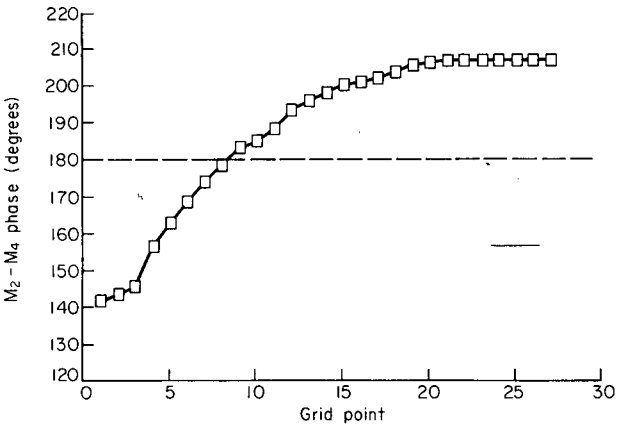

Figure 7. Adjustment in sea surface M_2–M_4 phase for model run 11 (compare with Figure 2). Below the dashed line, time asymmetry is characterized by a longer falling tide; above the line by a longer rising tide.

the forcing boundary ($\Phi_\zeta < 180°$). Where tidal flats are important, this inequality is reversed moving downchannel (compare Figures 2 and 7). Thus, large storage regions adjacent to the channel can produce a duration asymmetry characterized by a longer rising tide.

Harmonic growth and particularly the relative phase of M_4 in sea surface depend on the size of tidal flats, time variability of channel geometry and the level of friction. The first six experiments listed in Table 2 involve rectangular (i.e. 'weakly' time-variable) channels with different tidal flat areas and levels of friction. The geometry is similar to experiment 10 (Table 1) which has a longer falling than rising tide ($\Phi_\zeta \simeq +80°$). The addition of tidal flats to this channel geometry results in a longer rising tide (i.e. Φ_ζ between 180° and 360°). As the channel geometry becomes more time-variable (through larger a/h), the phase approaches 180°. For these experiments, a longer falling tide at the model's interior boundary does not occur.

The spectral structure of sea surface at grid point 26 and velocity at grid point 12 for experiments 10, 11 and 11A shows that the tidal flats experiments have a more non-linear response (Figure 8). The vigorous harmonic growth is caused by the larger velocities associated with experiments 11 and 11A. Harmonic analysis of the primary non-linear forcing terms, friction and continuity, for experiments 10 and 11A reveals the difference in non-linear response. With large dissipation of both mean velocity and sea surface near the forcing boundary, the continuity term in 11A drives strong M_4 and M_6 constituents. This term is a weaker source of non-linear forcing in experiment 10. Conversely, the friction term in experiment 10, while having a smaller absolute magnitude, nevertheless is a more non-linear term as measured by the M_4/M_2 ratio.

The next group of experiments listed in Table 2 introduces the effects of more time-variable channel geometry with variable friction and tidal flat area. The channel geometry is essentially the same as that used in experiment 13 (Table 1). Tidal asymmetries developed in these experiments reflect the conflicting effects of time-variable channel geometry in continuity and momentum tending to drive a longer falling tide and the presence of tidal flats in continuity driving a longer rising tide. As a result, a variety of channel responses including both types of time asymmetry is found. Sea surface phase adjustment between M_2 and M_4 can be substantial, particularly for experiments

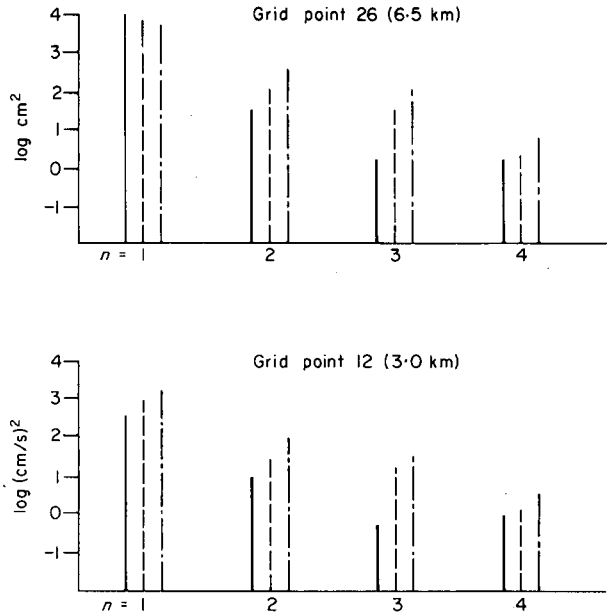

Figure 8. Periodogram of sea surface and velocity for three models showing the effect of increasing tidal flats area on the spectrum of the estuarine tidal response. ——, experiment no. 10; – – –, 11A; — · —, 11.

involving a mixture of large tidal flats and strongly time-variable geometry (e.g. experiment 14). The phase relationship of both sea surface and mean velocity shown in Table 2 is taken from near the interior model boundary and indicates the sense of tidal asymmetry the model is developing.

In general, most of these experiments have a longer falling tide ($\Phi_\zeta < 180°$), although the actual phase is quite different from experiment 13. The size of tidal flat area has an important effect on the type of tidal asymmetry. Sea surface at grid point 26 for experiment 14 shows little time asymmetry, although considerable distortion is present. If the amount of tidal flat area is increased, the example of a longer rising tide is found (experiment 14A). Conversely, as the area of tidal flats declines, the behavior of the model becomes more similar to experiment 13, as one would expect (compare experiments 17B and 13).

The final three experiments listed in Table 2 also emphasize the interaction of channel geometry and tidal flats. The larger ratio of $\triangle b/b_0$ indicates greater time-variability of channel geometry. The channel geometry is the same as experiment 13A (Table 1). For these examples, the effects of variable channel geometry dominate the tidal response even if the tidal flat area is large (experiment 23A). The result is that all three examples have a tidal asymmetry characterized by a longer falling tide.

The magnitude of friction within a channel affects its tidal asymmetry, as seen by comparing experiments 14, 14B and 14C, where the friction factor was reduced while the geometry remained the same. Harmonic growth in sea surface increases slightly with increasing friction and the amount of tidal dissipation increases dramatically. The M_2–M_4 phase of sea surface shifts from a nearly symmetrical tide in experiment 14 to a longer rising tide as the level of friction decreases (Table 2). The level of friction cannot be reduced low enough to produce this result. Shallow estuaries with

strong tidal flows will be characterized by friction factors of approximately 10^{-2} as opposed to the values of $1–2 \times 10^{-3}$ widely used in estuarine and shelf models.

Although the modeling focused on the estuarine response to pure M_2 forcing, the effects of harmonics introduced in the boundary conditions were studied. The importance of estuarine geometry in determining tidal distortion must be compared with the role of harmonics entering the estuary through the inlet. Tidal harmonics can be generated on ebb-tide deltas (shallow platform shoals located oceanward of the inlet). Field evidence suggests that phase relationships and amplitudes of harmonics are modified as the tide propagates into the estuary (Robinson *et al.*, 1983; Aubrey & Speer, 1983). At Nauset, pressure sensor records from the ebb-tide delta indicate different sea surface M_2–M_4 phase than within the estuary (Φ_ζ ebb delta $\simeq 30°$; Φ_ζ estuary $\simeq 63°$).

To examine M_4 boundary forcing in a model estuarine channel two different values of Φ_ζ (64°, 179°) in the boundary condition were applied to the geometry of experiment 13 (Table 1). Introduction of a small amount of M_4 ($M_4/M_2 = 0{\cdot}033$) at a compatible phase in the forcing boundary condition eliminates the rapid estuarine phase adjustment and results in slightly greater M_4 growth. The phase, Φ_ζ, at the model's interior boundary is close to that of experiment 13. In contrast, the same amount of M_4 introduced at a phase, Φ_ζ, of 179° produces a different result. The M_2–M_4 phase changes dramatically, approaching the value of experiment 13 near the model's interior boundary, and the amplitude of M_4 first declines before growing downchannel. Thus the channel geometry in the model runs exerts an important control on tidal asymmetry regardless of the presence of harmonics at the open boundary.

A comparison of two different estuarine geometries

The previous sections identified important estuarine channel characteristics forcing different senses of asymmetry and different rates of harmonic growth. Models described in this section employ geometries representative of two estuaries along the U.S. east coast. The first model approximates the flood-dominated main tidal channel at Nauset inlet/estuary (MA). The second represents an ebb-dominated estuarine channel at Wachapreague inlet/estuary (VA). These numerical experiments do not attempt to predict conditions at the estuaries in question, since their complexity cannot be reproduced adequately by one-dimensional models. Geometry parameters used in the previous sections represent the general features of channels in these two estuaries.

Nauset Inlet is characterized by shallow (<3 m) tidal channels which lead to an unstable inlet with flood and ebb tide delta deposits. Tidal flats along the main drainage channel are located near the inlet mouth and consist of flood tide delta and barrier overwash deposits. The total extent of tidal flats is moderate ($\sim 40\%$ of surface area) in this system. Nauset is modeled by a channel of constant width and depth and includes a region of tidal flats near the forcing boundary. The area of flats bordering the channel decreases linearly to zero moving downchannel. Wachapreague Inlet is characterized by deeper (~ 5 m) tidal channels terminating in broad shallow bays. The bays represent extensive tidal flat deposits with large changes in water surface area over a tidal cycle. The inlet itself is stable and lacks flood tide delta deposits. Wachapreague is modeled by a deep channel with contracting width downchannel. Channel reaches near the interior boundary are bordered by large regions of tidal flats. Since these experiments do not represent exact matches between prototype and model geometry, an ensemble of runs, varying the geometry and friction parameters over plausible ranges for each estuary,

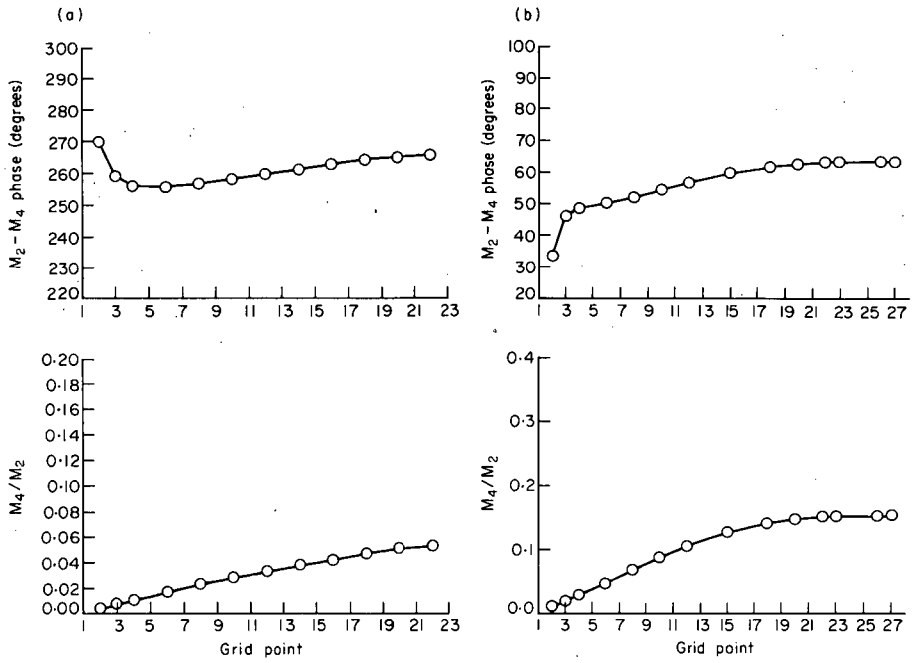

Figure 9(a). Summary of the tidal response of Wachapreague model W4. Top panel is sea surface M_2–M_4 phase adjustment. Lower panel is ratio of sea surface M_4/M_2 amplitudes. (b) Summary of the tidal response of Nauset model N1. Panels are the same as for Figure 9(a).

was considered. A consistent estuarine tidal response over a representative range of parameters was obtained. Two particular cases were selected to contrast features of the response for the two systems.

The models representing Wachapreague are characterized by a longer rising tide, stronger ebb flows and relatively weak harmonic growth [Figure 9(a)]. This result holds even if one allows for a trapezoidal channel geometry. The tidal response of the model is dominated by the presence of large tidal flat area and a relatively small a/h ratio ($\sim 0{\cdot}11$). Because of these factors, even strong friction (e.g. $f = 0{\cdot}020$) is unable to produce a longer falling tide. If the model is run without the tidal flats, harmonic growth is weak and sea surface phase produces a longer falling tide. Actual field measurements at Wachapreague show $(M_4/M_2)_\zeta$ equals approximately 0·04 within the estuary (Boon & Byrne, 1981). Sea surface phase is approximately 200–220°, producing a longer rising tide and stronger ebb currents. The simple model described in this section reproduces the general features of this tidal response by focusing on the 'first order' estuarine characteristics of Wachapreague.

The models representing Nauset display strong harmonic growth, a longer falling tide and stronger flood flows [Figure 9(b)]. The important factors determining its tidal response are the large a/h ratio ($\sim 0{\cdot}30$) which produces a strongly time-variable channel geometry and the moderate extent of tidal flats. The sea surface phase relationship ($\simeq 64°$) indicates that the effects of channel geometry dominate the effects of tidal flats. Field measurements at Nauset (Aubrey & Speer, 1985) show $(M_2/M_4)_\zeta$ is approximately 0·20 and Φ_ζ, 63°. Again, a simple representation of estuarine geometry (shallow tidal channels with moderate tidal flat area near the forcing boundary) has reproduced essential features of Nauset's tidal response.

Conclusions

(1) Numerical integration of the one-dimensional equations clarifies M_2 tidal propagation in narrow channels with tidal flats typically found in shallow estuaries along the U.S. east coast. Numerical results indicate that channels without tidal flats develop a time asymmetry characterized by a longer falling tide. This asymmetry becomes more pronounced with larger friction factors and increasingly time-variable channel cross-sectional area. Currents associated with this time asymmetry tend to be stronger during flood than ebb. These estuarine channels are termed flood-dominant.

(2) Addition of tidal flats to these channels can produce the case of a longer rising tide and stronger ebb currents (ebb-dominant). This time asymmetry develops if the tidal area is large enough to overcome the effects of time-variable channel geometry. Channels with relatively small values of a/h and rectangular cross-sections require smaller tidal flat area to produce an ebb-dominant asymmetry. It is difficult to parameterize the critical area of tidal flats which produces a longer rising tide because the modeling is only an approximate representation of estuarine physics, and sparse field evidence provides little guidance. Weaker values of friction with tidal flats can also drive the time asymmetry towards a longer rising tide.

(3) Despite the physical complexity of shallow estuarine systems, the general features of tidal channels in these estuaries can be represented with simple geometries. This is illustrated by modeling idealized representations of tidal channels at Nauset Inlet, MA, and Wachapreague Inlet, VA. Over a range of geometry parameters and friction factors which could characterize these estuaries, essential features of the estuarine tidal response in sea surface can be recovered.

(4) Field observations and model results suggest that the shallowest estuaries ($a/h > 0{\cdot}3$) generally will be characterized by longer falling tides and stronger flood currents unless extensive tidal flats are present. Deeper systems ($a/h \sim 0{\cdot}1$–$0{\cdot}2$) with tidal flats will likely have longer rising tides and stronger ebb currents. Near-bed sediment transport patterns in flood-dominant estuaries will be directed up-estuary with consequent channel shoaling if sediment supply is adequate. Ebb-dominant estuaries may represent more stable configurations with stronger ebb currents able to flush coarse sediments entering the estuary through the inlet. The behavior of suspended sediment is more complex, and is currently under investigation.

(5) The models considered here provide only qualitative information on the effects of tidal flats. To include these effects more accurately, the modeling must be extended to two dimensions (depth-integrated). Two-dimensional models solve the full momentum and continuity equations over the flats as well as in the channel. This enables the impact of tidal flats in momentum to be more carefully evaluated. Allowing greater cross-sectional area variability along channel and the possibility of channels in the tidal flats also requires a two-dimensional model. Given sufficient spatial resolution of estuarine geometry, two-dimensional models can also more accurately include regions where the advective term is of importance (e.g. channel bends, channel constrictions).

Acknowledgements

This study was partially supported by the Department of Commerce, NOAA Office of Sea Grant under grant numbers NA79AA–D–00102 and NA80AA–D–00077, the U.S.

Army Research Office under Grant DAAG 29–81–K–0004, the Woods Hole Oceanographic Institution's Coastal Research Center, and the W.H.O.I. education program. Wayne Spencer and Steven Gegg oversaw the field program. Pamela Barrows typed the manuscript. William D. Grant, Dale B. Haidvogel and John D. Milliman suggested improvements to the manuscript.

References

Aubrey, D. G. & Speer, P. E. 1983 Sediment transport in a tidal inlet. Woods Hole Oceanographic Institution Technical Report, WHOI 83–20, 130 pp.

Aubrey, D. G. & Speer, P. E. 1984 Updrift migration of tidal inlets. *Journal of Geology*, **92**, 531–545.

Aubrey, D. G. & Speer, P. E. 1985 A study of non-linear tidal propagation in shallow inlet/estuarine systems. Part I: Observations. *Estuarine, Coastal and Shelf Science*, **21**, 185–205.

Boon, J. D. III & Byrne, R. J. 1981 On basin hypsometry and the morphodynamic response of coastal inlet systems. *Marine Geology*, **40**, 27–48.

Byrne, R. J., DeAlteris, J. T. & Sovich, J. P. 1977 Recent history and response characteristics of Wachapreague Inlet, VA. Final report to ONR Geography Programs, VIMS, Gloucester Pt., VA. 127 pp.

Dronkers, J. J. 1964 *Tidal Computations in Rivers and Coastal Waters*. North Holland Publishing Company, Amsterdam. 516 pp.

FitzGerald, D. M. & Nummedal, D. 1983 Response characteristics of an ebb-dominated tidal inlet channel. *Jour. Sed. Pet.*, **53**, 833–845.

Flather, R. A. & Heaps, N. S. 1975 Tidal computations for Morecambe Bay. *Geophysical Journal of the Royal Astronomical Society*, **42**, 489–517.

Gallagher, B. S. & Munk, W. H. 1971 Tides in shallow water: spectroscopy. *Tellus*, **23**, 346–363.

Hamilton, J., 1978 The quarter-diurnal tide in the English Channel. *Geophysical Journal of the Royal Astronomical Society*, **53**, 541–552.

Kabbaj, A. & Le Provost, C. 1980 Non-linear tidal waves in channels: a perturbation method adopted to the importance of bottom friction. *Tellus*, **32**, 143–163.

Kjerfve, B. 1975 Velocity averaging in estuaries characterized by a large tidal range to depth ratio. *Estuarine and Coastal Marine Science*, **3**, 311–323.

Kreiss, H. 1957 Some remarks about nonlinear oscillations in tidal channels. *Tellus*, **9**, 53–68.

Nummedal, D. & Humphries, S. M. 1978 Hydraulics and dynamics of the North Inlet, 1975–1976. *G.I.T.I. Report 16*, US Army Coastal Engr. Res. Cent., 214 pp.

Owen, A. 1980 The tidal regime of the Bristol Channel: a numerical modeling approach. *Geophysical Journal of the Royal Astronomical Society*, **62**, 59–75.

Pingree, R. D. & Griffiths, D. K. 1979 Sand transport paths around the British Isles resulting from M_2 and M_4 tidal interactions. *Journal of the Marine Biological Association of the United Kingdom*, **59**, 497–513.

Pingree, R. D. & Maddock, L. 1978 The M_4 tide in the English channel derived from a nonlinear numerical model of the M_2 tide. *Deep-sea Research*, **26**, 53–68.

Prandle, D. 1980 Modeling of tidal barrier schemes: an analysis of the open-boundary problem by reference to AC circuit theory. *Estuarine and Coastal Marine Science*, **11**, 53–71.

Robinson, I. S., Warren, L. & Longbottom, J. F. 1983 Sea-level fluctuations in the Fleet, an English tidal lagoon. *Estuarine, Coastal and Shelf Science*, **16**, 651–668.

Smith, J.D. & McLean, S. R. 1983. A model for meandering streams. *Water Resources Research*.

Speer, P. E., 1984 *Tidal distortion in shallow estuaries*. Ph.D. thesis, WHOI-MIT Joint Program in Oceanography, Woods Hole, MA. 210 pp.

Speer, P. E. & Aubrey, D. G. in prep. Momentum balances and tidal bottom stress in a shallow estuary.

Swift, M. R. & Brown, W. S. 1983 Distribution of tidal bottom stress in a New Hampshire estuary. Report No. UNH–MP–T/DR–SG–83–2, Univ. of New Hampshire. 40 pp.

Teubner, M. D. & Noye, B. J. 1978 Tidal and thermal propagation in a tidal estuary. In *Numerical Simulation of Fluid Motion* (Noye, J., ed.). North-Holland, Amsterdam. 580 pp.

Uncles, R. J. & Jordan, M. B. 1980 A one-dimensional representation of residual currents in the Severn Estuary and associated observations. *Estuarine and Coastal Marine Science*, **10**, 39–60.